HOXD1 inhibits lung adenocarcinoma progression and is regulated by DNA methylation

XIN HU[1], SIJIA ZHANG[1], XIAOYU ZHANG[1], HONGYAN LIU[2], YUTAO DIAO[1] and LIANLIAN LI[1,3]

[1]Department of Immunology, School of Clinical and Basic Medical Sciences, Shandong First Medical University, Jinan, Shandong 250117, P.R. China; [2]Research Center of Basic Medicine, Jinan Central Hospital, Shandong First Medical University, Jinan, Shandong 250013, P.R. China; [3]Department of Oncology, Shandong Provincial Hospital Affiliated to Shandong First Medical University, Jinan, Shandong 250021, P.R. China

Abstract. The homeobox (HOX) gene family encodes a number of highly conserved transcription factors and serves a crucial role in embryonic development and tumorigenesis. Homeobox D1 (HOXD1) is a member of the HOX family, whose biological functions in lung cancer are currently unclear. The University of Alabama at Birmingham Cancer data analysis Portal of HOXD1 expression patterns demonstrated that HOXD1 was downregulated in lung adenocarcinoma (LUAD) patient samples compared with adjacent normal tissue. Western blotting analysis demonstrated low HOXD1 protein expression levels in lung LUAD cell lines. The Kaplan-Meier plotter database demonstrated that reduced HOXD1 expression levels in LUAD correlated with poorer overall survival. Meanwhile, an *in vitro* study showed that HOXD1 overexpression suppressed LUAD cell proliferation, migration and invasion. In a mouse tumor model, upregulated HOXD1 was demonstrated to inhibit tumor growth. In addition, targeted bisulfite sequencing and chromatin immunoprecipitation assays demonstrated that DNA hypermethylation occurred in the promoter region of the HOXD1 gene and was associated with the action of DNA methyltransferases. Moreover, upregulated HOXD1 served as a transcriptional factor and increased the transcriptional expression of bone morphogenic protein (BMP)2 and BMP6. Taken together, the dysregulation of HOXD1 mediated by DNA methylation inhibited the initiation and progression of LUAD by regulating the expression of BMP2/BMP6.

Introduction

Lung cancer has high morbidity (~12.4% of new cases of cancer) and mortality (~18.7% of cancer deaths) rates, making it the leading cause of cancer deaths globally (1-3). Lung cancer is categorized into small cell lung cancer and non-small cell lung cancer (NSCLC) including lung squamous carcinoma, lung adenocarcinoma (LUAD) and lung large cell carcinoma, of which NSCLC is the predominant histologic type (3). Although there have been considerable advancements in the early detection strategies of NSCLC, such as early screening and minimally invasive diagnostics, and in the treatment of NSCLC with radiation therapy, targeted therapies against disease-associated oncogenic driver molecules and immunotherapies related to immune checkpoint inhibitors, the identification of emerging biomarkers is important for guiding the prognosis of NSCLC (4,5). Understanding the molecular carcinogenesis and studying oncogenic drivers can greatly aid in the development of targeted therapeutics for NSCLC and provide additional treatment options, thereby increasing patient survival.

Homeobox (HOX) genes are a highly conserved family of genes encoding a type of DNA-binding transcription factor, which are involved in cell differentiation, metastasis and angiogenesis (6). Mammals have 39 HOX genes arranged into four clusters: A, B, C and D (7,8). Previous research showed that aberrant HOX gene expression has a role in the progression of certain types of cancer, such as breast cancer (9), lung cancer (10) and glioblastoma (11). HOXD, located on chromosome 2q31, is a subfamily of HOX genes (12) and includes HOXD1, D3, D4, D8, D9, D10, D11, D12 and D13 genes (13). In lung cancer research, the HOXD3 pro-oncogene enhances lung adenocarcinoma cell metastasis by downregulating E-cadherin and upregulating N-cadherin, as well as facilitating tumor

invasion and angiogenesis by influencing urokinase-type plasminogen activator and MMP-2 expression (14). Similarly, in A549 cells, a loss of microRNA (miR)-520a-3p causes overexpression of HOXD8, which enhances cell proliferation and cancer cell stemness (15). Overexpressed HOXD9 has also been reported to target the 6-phosphofructo-2-kinase/fructose-2,6-biphosphatase 3 promoter region, which may lead to malignant behavior in NSCLC (16). Moreover, miR-224 can participate in NSCLC progression via regulating HOXD10 expression (17). In summary, dysregulation of the HOXD genes is associated with the occurrence and progression of lung cancer. However, to the best of our knowledge, there have been no reports regarding the role of HOXD1 in the occurrence and development of lung cancer to date.

Epigenetic control is the most prevalent method in HOX gene regulation (18), and abnormal DNA methylation levels of certain HOX gene promoters have been identified in cancer studies (8). For example, peripheral blood DNA methylation profiles showed hypermethylation of the HOX gene CpG region in non-Hodgkin lymphoma (19). Furthermore, the promoters of HOXB5 and HOXB7 have been shown to exhibit hypomethylation levels, which increases the metastasis of small cell lung cancer (20). Between 60-90% of the CpGs in the genome are methylated, and the unmethylated CpGs are clustered into CpG islands in the promoter and exon regions of structural genes (21). Therefore, an abnormal methylation status in the CpG islands can lead to the onset of cancer. The hypermethylation of the tumor suppressor gene CpG islands inhibits gene transcription, resulting in the loss of an anti-cancer effect (21,22). Hypermethylation of various genes in the HOXD family, including HOXD3, HOXD10 and HOXD13, has also been identified in lung cancer (8). There are three main catalytic DNA methyltransferases (DNMTs), DNMT1, DNMT3A and DNMT3B, involved in the DNA methylation process (23). It has been reported that normal DNA methylation levels are impacted by DNMT dysregulation. A previous study reported that DNMT1/3A/3B are overexpressed in oral squamous cell carcinoma, which triggers promoter hypermethylation silencing of >40 cancer-suppressor genes (24). In addition, overexpression of DNMT1/3A in prostate cancer accelerates cancer progression by epigenetic silencing of Claudin-1 (25). In summary, DNA methylation of certain HOX genes has been reported to occur in lung cancer and to contribute to the development of cancer. However, reports on the mechanism of DNA methylation control of HOXD1 in LUAD re currently limited.

In the present study, the objective was to investigate the function of HOXD1 and its regulation mechanisms in the initiation and development of LUAD. Through the exploration, this study aimed to reveal the potential of HOXD 1 as a molecular target for clinical treatment of LUAD, providing theoretical basis for early diagnosis and treatment of LUAD. The present findings promoted the promise of novel and impactful therapeutic strategies for LUAD.

Materials and methods

Differential expression gene analysis and prognostic value in LUAD. The expression of nine HOX genes of the HOXD cluster in LUAD tissues and normal tissues were examined using The University of Alabama at Birmingham Cancer data analysis Portal (UALCAN) database (http://ualcan.path.uab.edu/analysis-prot.html) (26). The prognostic value of HOXD1 expression for overall survival (OS), first progression (FP) and post-progression survival (PPS) was analyzed using the Kaplan-Meier plotter (http://kmplot.com) (27).

Cell culture. The human normal lung epithelial cell line (BEAS-2B) and LUAD cell lines (A549, H1299, H1650 and H1975) were purchased from Cell Bank/Stem Cell Bank, Chinese Academy of Sciences. BEAS-2B and A549 were cultured in DMEM (Shanghai VivaCell Biosciences, Ltd.) supplemented with 1% penicillin/streptomycin (Beijing Solarbio Science & Technology Co., Ltd.) and 10% FBS (CellMax). H1299, H1650 and H1975 cells were cultured in RPMI 1640 (Shanghai VivaCell Biosciences, Ltd.) supplemented with 1% penicillin/streptomycin (Beijing Solarbio Science & Technology Co., Ltd.) and 10% FBS. All cells were cultured at 37°C and 5% CO_2.

Virus production and infection. The lentiviruses used in this study were produced by Shanghai GeneChem Co., Ltd. Lentiviruses expressing HOXD1 were produced using the lentiviral vector GV492 (Shanghai GeneChem Co., Ltd.). The virus transfection process was performed according to manufacturer's protocol. Briefly, A549 or H1299 cells were seeded at $3-5x10^4$ cells/ml in 6-well plates. Lentiviruses containing the negative control (LV-NC; empty lentiviral vector GV-492) or HOXD1 vector (LV-HOXD1) were transfected into A549 or H1299 cells (multiplicity of infection, 10). The volume of culture medium was 1 ml/well in 6-well plates and 1X HitransG P (Shanghai GeneChem Co., Ltd.) was added to each well and incubate for 14-26 h at 37°C and 5% CO_2, the medium was replaced with fresh complete culture medium. Puromycin (6 μg/ml) selection was then used for 2 days and 3 μg/ml puromycin was used for maintenance to produce stably transfected cells.

Xenograft mouse model. A total of 16 female BALB/cA-nu mice (weight, 18-20 g; age, 4-5-weeks; Beijing HFK Bioscience Co., Ltd.,) were housed under specific pathogen-free conditions. The mice had *ad libitum* access to food/water and were housed under a 12 h light/dark cycle. The temperature was maintained at 24±2°C and a relative humidity range of 50-60% was maintained. All procedures were approved by the Animal Use and Care Committee at Shandong Provincial Hospital Affiliated with Shandong First Medical University (approval no. 2021-622; Jinan, China). A549 cells transfected with either the LV-NC or LV-HOXD1 plasmid vector via lentiviruses were used in the tumor formation assay. The nude mice were divided into two groups (8 mice/group): LV-NC and LV-HOXD1. All mice were injected subcutaneously in the right hind limb with $3x10^6$ A549 LV-NC or LV-HOXD1 cells in 150 μl PBS. The experimental duration of the present study was 5 weeks, with the first week allocated for adaptive feeding. The experiment commenced at the beginning of the second week, with the subcutaneous injection of cells to establish a xenograft tumor animal model. Animal health was observed daily and the body weight of the mice and tumor diameters were measured weekly for 4 weeks. If any humane endpoints were reached, the animals were sacrificed. These

included a tumor diameter >20 mm, weight loss >20% of body weight, the animal exhibited cachexia or wasting syndrome or the size of the solid tumor >10% of body weight. Notably, none of the mice succumbed to humane endpoints during the experimental process. The mice were euthanized by cervical dislocation. Tumors were then dissected and tumor weights were measured.

Small interfering (si)RNA transfection. The siRNAs (siR) used in the present study were constructed by external companies (siR-DNMTs, Guangzhou RiboBio Co., Ltd.; siR-NC, Shanghai GenePharma Co., Ltd.). A549 cells were incubated with 10 μM siR-DNMTs (Guangzhou RiboBio Co., Ltd.) and siR-negative control (siR-NC) (Shanghai GenePharma Co., Ltd.) using Lipofectamine® RNAiMAX Reagent (cat. no. 13778-150; Invitrogen; Thermo Fisher Scientific, Inc.) (Table SI). An equal concentration of siR-NC was added to A549 cells as a control. Cells were seeded in 6-well plates until they reached 40-50% confluence. To prepare the transfection mix according to the manufacturer's protocol, 9 μl Lipofectamine® RNAiMAX was diluted in 150 μl Opti-MEM Medium (Gibco; Thermo Fisher Scientific, Inc.) and mixed. Additionally, 3 μl siRNA was diluted in 150 μl Opti-MEM Medium and mixed separately. The diluted siRNA was then mixed with the diluted Lipofectamine® RNAiMAX in a 1:1 ratio to form a siRNA-lipid complex. This complex was incubated for 5 min at room temperature before being added to the cultured cells. Following transfection, the cells were incubated at 37°C. After 48 h of transfection, the medium was removed from the wells. Cells were washed 3 times with cold PBS and then 500 μl RNAiso Plus reagent (Takara Bio, Inc.) was added to thoroughly lyse cells using RNase-Free Pipette Tips.

RT-qPCR. Total RNA was extracted from BEAS-2B cells and the LUAD cell lines, A549 cells transfected with siR-NC or with siR-DNMTs, and A549 and H1299 cells transfected with lentiviruses containing the negative control (LV-NC) or HOXD1 (LV-HOXD1) vector using RNAiso Plus reagent (Takara Bio, Inc.) according to the manufacturer's instructions. The RNA pellet was recovered in RNase-free water and the RNA concentration and purity were measured using the NanoDrop 1000 (Thermo Fisher Scientific, Inc.). cDNA was synthesized using the Evo M-MLV RT Premix (Hunan Accurate Bio-Medical Technology Co., Ltd.) according to the manufacturer's protocol. The cDNA was used as the template for RT-qPCR using the Taq SYBR Green qPCR Premix (Jiangsu Best-Enzymes Biotechnology Co., Ltd.). The following thermocycling conditions were used for qPCR: Initial denaturation at 95°C for 10 sec; 40 cycles of 60°C for 10 sec and 72°C for 30 sec. The final results were analyzed as previously described (28) and the relative quantification of target genes were analyzed using the $2^{-\Delta\Delta Cq}$ method (29) after normalization to β-actin or GAPDH expression levels. The primers used are listed in Table SII.

Western blotting. Cells were lysed on ice using RIPA lysis buffer (New Cell & Molecular Biotech Co., Ltd.) containing Protease Inhibitor Cocktail (New Cell & Molecular Biotech Co., Ltd.). Protein concentrations in the samples were quantified using the NanoDrop 1000 (Thermo Fisher Scientific, Inc.).

A total of 75 μg protein/lane were separated by SDS-PAGE electrophoresis using a 10-12.5% gel, followed by transfer to PVDF membranes (cat. no. IPVH00010; MilliporeSigma). After blocking in 5% skim milk for 2 h at room temperature, the membranes were incubated with primary antibodies against HOXD1 (1:500; cat. no. ab220856; Abcam), Flag M2 (1:5,000; cat. no. m20008m; Abmart Pharmaceutical Technology Co., Ltd.) and GAPDH (1:50.000; cat. no. 60004-I-Ig; Proteintech Group, Inc.) overnight at 4°C. After washing three times with TBST containing 0.1% Tween-20, the membranes were incubated with anti-mouse IgG HRP-linked antibodies (1:20,000; cat. no. AB0102; Shanghai Abways Biotechnology Co., Ltd.) and anti-rabbit IgG HRP-linked antibodies (1:50,000; cat. no. AB0101; Shanghai Abways Biotechnology Co., Ltd.) at room temperature for 1 h and an ECL kit (cat. no. WBKLS0500; MilliporeSigma) were used for visualization. The chemiluminescence imaging system (ChemiDoc M, Bio-Rad Laboratories, Inc.) was used for imaging and ImageJ software (version 1.51j8; National Institutes of Health,) was used for semi-quantitation of protein levels. GAPDH was used as a reference control.

Methylation analysis. The UALCAN database was used to analyze HOXD1 promoter methylation levels (26). CpG islands in the HOXD1 promoter sequence were predicted using MethPrimer (http://www.urogene.org/methprimer/) (30). TBS was performed by Igenebook Biotechnology Co., Ltd. Briefly, bisulfite sequencing PCR primers targeting the HOXD1 promoter region were designed using MethPrimer (Table SIII). The HOXD1 promoter region was selected from upstream 2,000 bp to downstream 1,000 bp of the transcription start site (TSS) and located on the National Center for Biotechnology Information (https://www.ncbi.nlm.nih.gov/) nucleotide sequence starting from 176,186,579 and ending at 176,189,579 (accession no. NC_000002). Genomic DNA from BEAS-2B, A549 and H1299 cells were extracted and bisulfite treatment was performed using the EZ DNA Methylation-Gold™ Kit (cat. no. D5005; Zymo Research Corp.). DNA quality was detected using the Qubit 4.0. Bisulfite-treated templates were subjected to bisulfite sequencing PCR (BSP) amplification by high-fidelity U-base-resistant DNA polymerase BSP amplification. BSP amplification products from the same sample were mixed and labeled primers were amplified to obtain a bisulfite-converted DNA library. The library from each sample was pooled and sequenced using the Illumina NovaSeq6000 platform (Illumina, Inc.) using the paired end 150 bp method as previously described (31,32). A library concentration of 13.1 ng/μl was measured using Qubit 4.0. Trimmomatic (version 0.36), BSMAP (version v2.7.3) and FastQC (version 0.11.7; https://www.bioinformatics.babraham.ac.uk/projects/fastqc/) were used for data analysis (33,34).

Decitabine treatment. A549 cells at a density of 70-80% were treated with 0.1, 1.0, 5.0 or 10.0 μM decitabine [5-aza-2'-deoxycytidine (DAC); cat. no. ID0120; Beijing Solarbio Science & Technology Co., Ltd.] and 10 μM DMSO (cat. no. D8371; Beijing Solarbio Science & Technology Co., Ltd.) for 96 h at 37°C and 5% CO_2. The cells were then collected for RNA extraction and RT-qPCR analysis.

Cell proliferation assay and colony formation assay. Cell proliferation was measured using crystal violet staining, Cell Counting Kit-8 (CCK-8) and colony formation assays. For the crystal violet staining assay, cells were seeded in a 12-well culture plate at $1x10^5$ cells/well and incubated for 3 days. After washing twice with cold PBS, cells were fixed using 5% glacial acetic acid for 15 min at room temperature and then stained with 0.1% crystal violet for 10 min at room temperature. Cells were imaged using a camera. For the CCK-8 assay, it was performed according to manufacturer's protocol of CCK-8 reagent (cat. no. BS350B; Biosharp Life Sciences). Briefly, cells were seeded in a 96-well culture plate at a density of $2\text{-}3x10^3$ cells/well. After the cells were adherent and were cultured for different time periods (0, 24, 48 and 72 h), 10 μl/well of CCK-8 reagent was added, and then the cells were incubated for 2 h at 37°C and 5% CO_2. Absorbance at 450 nm was measured using a microplate reader (SpectraMax 190; Molecular Devices, LLC). For the colony formation assay, cells were seeded at a density of $1x10^3$ cells/well in a 6-well culture plate and incubated for 7 days until a single cell proliferated to form a visible cluster which was defined as a colony. After discarding the culture medium and washing twice with PBS, 4% paraformaldehyde was added to each well to fix the cells for 30 min at room temperature. Then, cells were stained with 2 ml of 0.1% crystal violet for 3 min at room temperature. Visible colonies were counted using Image J software.

Wound healing and Transwell assays. For the wound-healing assay, $1x10^6$ A549 cells were seeded in a 6-well plate and then scratched with a 10 μl pipette tip. The cells were washed 3 times with PBS to remove the scratched cells and then serum-free medium (DMEM or RPMI 1640) was used to culture the cells. Cells were cultured at 37°C and 5% CO_2. The migration of cells at the indicated time points of 0 and 96 h was observed using an inverted fluorescence microscope (Olympus IX73; Olympus Corporation). The width of the wound was measured using Photoshop (version 2017.1.6; Adobe Systems, Inc.). For the Transwell experiments, Transwell inserts were used with or without a Matrigel coating (cat. no. HY-K6001; MedChemExpress) for the cell invasion and migration experiments. Matrigel was melted at 4°C overnight and diluted with pre-cooled serum-free medium at 4°C to a final concentration of 1 mg/ml and maintained on ice. Then, 100 μl of diluted Matrigel was added to the center of the bottom of the upper chamber and incubated at 37°C for 4-5 h to dry. Control cells (A549 LV-NC and H1299 LV-NC) and HOXD1-overexpression cells (A549 LV-HOXD1 and H1299 LV-HOXD1) were seeded at a density of $2x10^5$ cells in the upper chamber in serum-free medium. Regular culture medium containing 10% FBS was added to the lower chamber. Cells were then incubated at 37°C for 24 h. Migratory and invasive cells in the lower chambers were stained using 0.1% crystal violet for 2 min at room temperature. Finally, cells were imaged using a light microscope (Olympus IX73; Olympus Corporation). Cells were counted and photographed in three randomly selected fields of view and quantified using Image J software.

ChIP-seq and ChIP-qPCR. The ChIP assays were conducted by Igenebook Biotechnology Co., Ltd. Briefly, ~$3x10^7$ A549 cells were washed twice in cold PBS, cross-linked with 1%

formaldehyde for 10 min at room temperature, quenched with glycine for 5 min at room temperature and then washed twice with cold PBS at room temperature. Cells were collected by centrifugation at 1,000 x g for 5 min at 4°C. Samples were lysed using 50 mM Tris-HCl (pH 8.0), 10 mM EDTA, 1% SDS, 1X protease inhibitor cocktail (cat. no. 5056489001; MilliporeSigma) and chromatin on ice. The chromatin was sheared into an average DNA fragment length of 200-500 bp. Additionally, 20 μl of chromatin was stored at -20°C for input DNA and 100 μl chromatin was incubated at 4°C overnight with antibodies against Flag M2 (1:50; cat. no. 14793; Cell Signaling Technology), DNMT1 (1:100; cat. no. 24206-1-AP; Proteintech), DNMT3A (1:100; cat. no. 20954-1-AP; Proteintech), DNMT3B (1:50; cat. no. 26971-1-AP; Proteintech) or IgG (1:100; cat. no. 2729S; Cell Signaling Technology, Inc.) as a negative control for immunoprecipitation. Then, 30 μl of protein beads (Dynabeads™ protein G; cat. no. 10004D; Thermo Fisher Scientific, Inc.) were added and the samples were further incubated for 3 h at 4°C. The beads were then washed once with 20 mM Tris/HCL (pH 8.1), 50 mM NaCl, 2 mM EDTA, 1% Triton X-100 and 0.1% SDS, washed twice with 10 mM Tris/HCL (pH 8.1), 250 mM LiCl, 1 mM EDTA, 1% NP-40 and 1% deoxycholic acid and twice with 1X TE buffer (10 mM Tris-Cl at pH 7.5 and 1 mM EDTA). Bound material was then eluted from the beads using 300 μl of elution buffer (100 mM NaHCO3 and 1% SDS), treated with RNase A (8 μg/ml; cat. no. EN0531; Thermo Fisher Scientific, Inc.) for 6 h at 65°C and then with proteinase K (345 μg/ml; cat. no. P6556; MilliporeSigma) overnight at 45°C. DNA concentration and purity were detected using the Q-bit (Qbit 4.0; Invitrogen; Thermo Fisher Scientific, Inc.). The purified products were used to construct sequencing libraries following the protocol provided by the I NEXTFLEX® ChIP-Seq Library Prep Kit for Illumina® Sequencing (cat. no. NOVA-5143-02, Bioo Scientific). The concentration of the libraries were assayed using the Qubit 4.0 and the fragment size determined using the QSep400 (Bioptic). The library concentration of 22.5 nM was determined by qPCR. Then, the purified products were sequenced on an Illumina NovaSeq using the paired end 150 bp method (35). Trimmomatic (version 0.36) was used to filter out low-quality reads. Next, clean reads were mapped to the human genome using BWA (version 0.7.15-r1140). Samtools (version 1.3.1) was used to remove potential PCR duplicates. MACS2 software (version 2.1.1.20160309) was adopted to screen peaks (bandwidth 300 bp; model fold 5, 50; q value 0.05). Peaks were assigned to genes if their midpoint was closest to the TSS of a single gene (36). HOMER (version 3) was used to predict motif occurrences within peaks with default settings for a maximum motif length of 12 bp (37). The ClusterProfiler (http://www.bioconductor.org/packages/release/bioc/html/clusterProfiler.html) R package (38) was employed to perform Gene Ontology (GO; http://geneontology.org/) (39) and Kyoto Encyclopedia of Genes and Genomes (KEGG; http://www.genome.jp/kegg/) (40) enrichment analyses. The GO and KEGG enrichment analyses were calculated using hypergeometric distribution with a q value cutoff of 0.05.

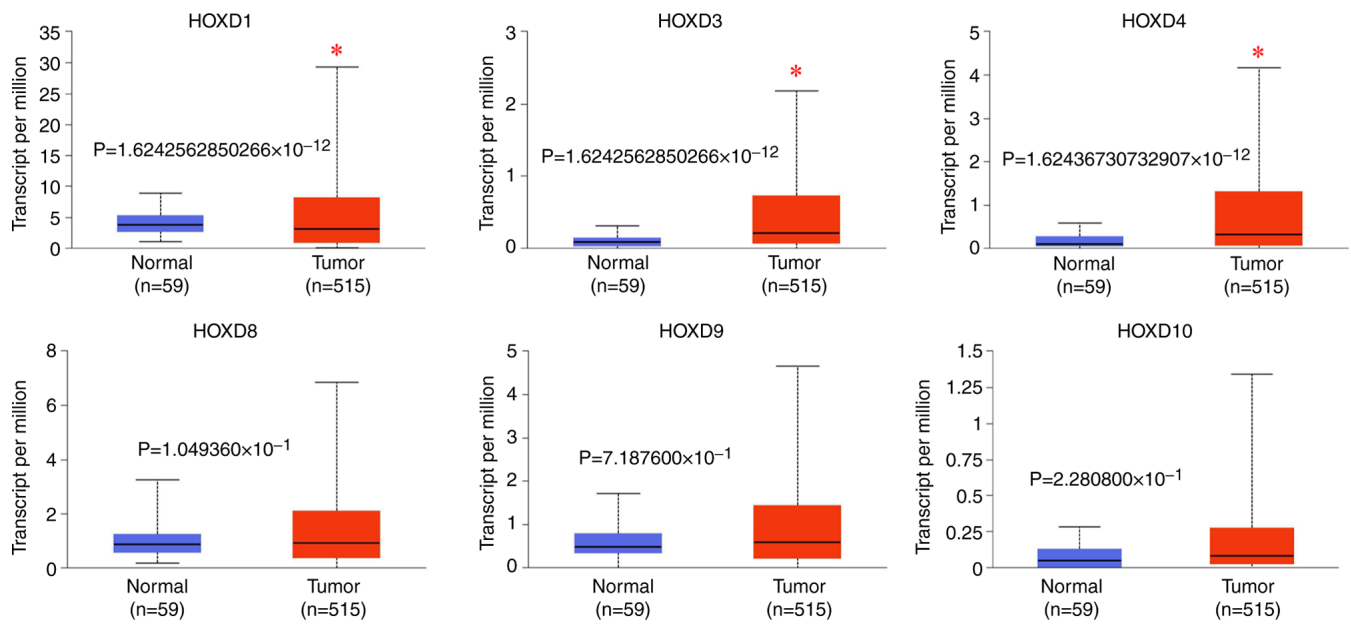For ChIP-qPCR, the extracted DNA fragments were used as templates for qPCR analysis using the ChamQ SYBR Color

Figure 1. mRNA expression levels of HOXD genes in lung adenocarcinoma were analyzed using The University of Alabama at Birmingham Cancer data analysis Portal database. Data were presented as mean ± SD. *P<0.05 vs. normal. HOX, homeobox.

qPCR Master Mix (cat. no. Q411; Vazyme Biotech Co., Ltd.). The 2,000 bp region upstream of the TSS in the HOXD1 promoter region was divided into seven segments (F1, F2, F3, F4, F5, F6 and F7), and primers were designed for each segment. Primers are listed in Table SIV. The following thermocycling conditions were used for qPCR: Initial denaturation at 95°C for 30 sec; 40 cycles of 95°C for 10 sec and 60°C for 30 sec. The data were normalized to the input. The final results were analyzed as previously described (28) and the relative quantification of target genes were analyzed using the $2^{-\Delta\Delta Cq}$ method (29).

Statistical analysis. Differential expression data for the HOXD family in lung adenocarcinoma derived from the UALCAN database were analyzed using Welch's t-test. Survival analyses from the Kaplan-Meier Plotter database were conducted using Cox regression analysis. All experiments were repeated at least three times. GraphPad Prism software (version 8.0.1; Dotmatics) was used for all statistical analyses. A student's t-test was used to analyze the colony formation, Transwell and xenograft tumor assays and the differential expression of BMP2 and BMP6. The CCK-8 assay data were analyzed using a two-way ANOVA followed by Bonferroni's post hoc test. HOXD1 expression in lung adenocarcinoma cell lines and data from the DAC treatment experiments were analyzed using one-way ANOVA followed by Dunnett's post hoc test. The ChIP-qPCR results were analyzed using a two-tailed unpaired Student's t-test. Data were presented as mean ± SD. P<0.05 was considered to indicate a statistically significant difference.

Results

HOXD1 was downregulated in LUAD and low expression levels predicted poor patient prognosis. The UALCAN database was used to examine the expression levels of nine HOX genes from the HOXD cluster in LUAD (Fig. 1). It was demonstrated that HOXD1 expression level in the tumor group (median level, 3.125) was significantly lower compared with that in the normal group (median level, 3.735) (P<0.05), while HOXD3 (median level of tumor group, 0.211; median level of normal group, 0.084) and HOXD4 (median level of tumor group, 0.317; median level of normal group, 0.097) expression levels were significantly increased in the tumor groups compared with the normal groups (P<0.05). There were no significant differences in HOXD8 (median level of tumor group, 0.903; median level of normal group, 0.864) (P>0.05), HOXD9 (median level of tumor group, 0.582; median level of normal group, 0.47) (P>0.05) and HOXD10 (median level of tumor group, 0.082; median level of normal group, 0.049) (P>0.05) expression levels between the tumor and normal groups. There were no data for the expression of HOXD11, HOXD12 and HOXD13 in the samples analyzed. In addition, HOXD1 expression levels were demonstrated to be low in LUAD cell lines compared with a normal lung epithelial cell line (Fig. 2A and B).

The prognostic values of the HOXD1 gene in patients with LUAD were analyzed using Kaplan-Meier plotter. It was demonstrated that patients with LUAD who had lower expression levels of HOXD1 had a poorer predicted OS (P=0.0014) and FP (P=0.00023) compared with patients with high expression levels of HOXD1, whereas there was no difference in PPS between the two patient groups (P=0.4) (Fig. 2C). These data indicated that HOXD1 expression was downregulated in LUAD in comparison to the normal lung, and low HOXD1 expression levels may be associated with a poor prognosis in patients with LUAD.

HOXD1 suppressed LUAD progression in vivo and in vitro. To explore the function of HOXD1 in LUAD, two stably transfected cell lines (A549 and H1299) overexpressing HOXD1 were established. A549 and H1299 cells were transfected with LV-NC and LV-HOXD1 to establish HOXD1 overexpression
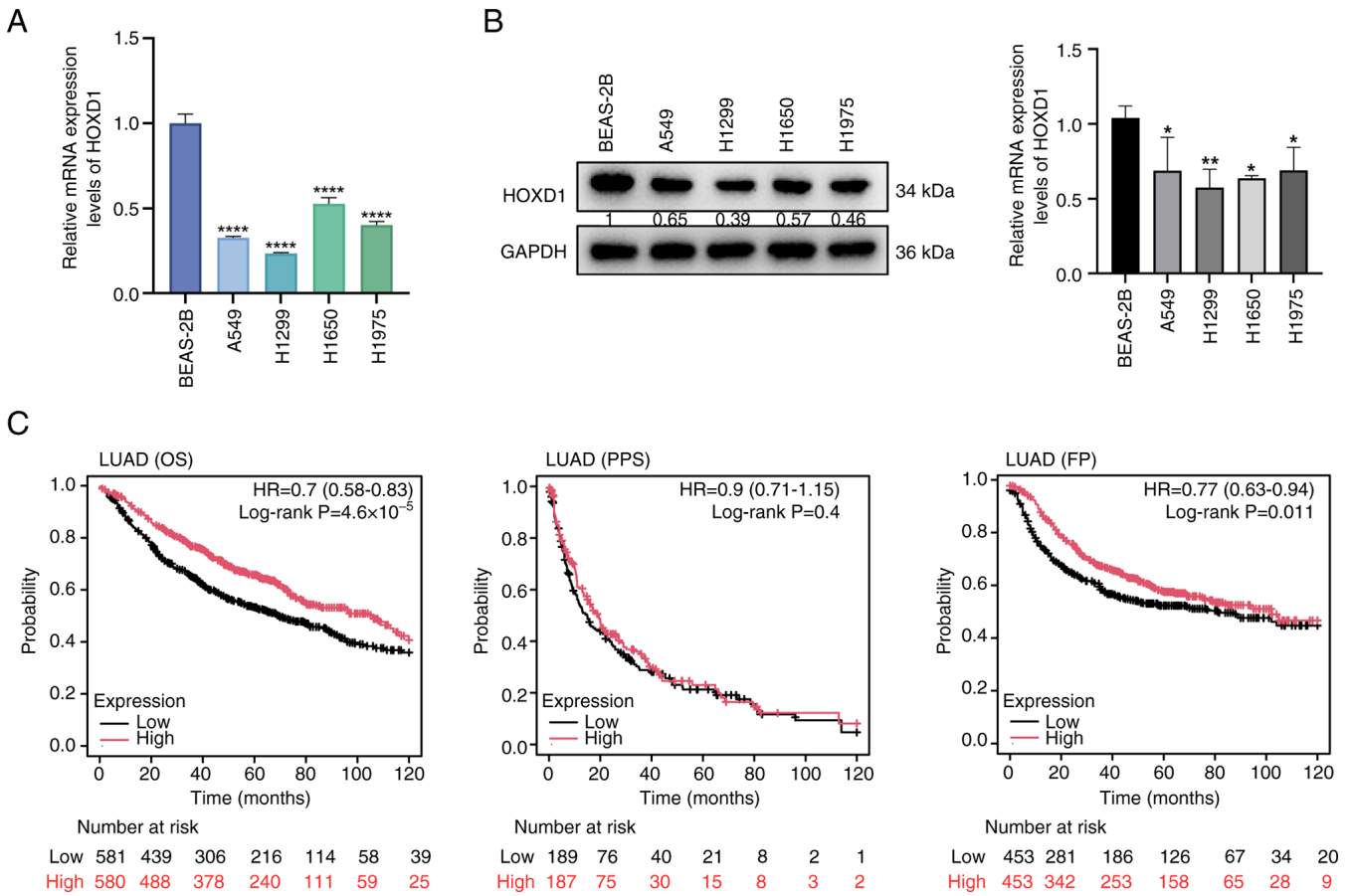
Figure 2. Expression of HOXD1 in lung adenocarcinoma cell lines and its correlation with survival. The relative (A) mRNA and (B) protein expression levels of HOXD1 were detected in LUAD cell lines by reverse transcription-quantitative PCR and western blotting, respectively. The numbers referred to the semi-quantitation of protein expression levels. (C) Prognostic values of *HOXD1* expression for OS, PPS and FP in patients with LUAD were analyzed using the Kaplan-Meier plotter. Data were presented as mean ± SD. *P<0.05, **P<0.01, ****P<0.0001 vs. BEAS-2B. HOX, homeobox; LUAD, lung adenocarcinoma; OS, overall survival; PPS, post-progression survival; FP, first progression.

cell lines (Fig. 3A). Crystal violet staining, CCK-8 assays and colony formation assays demonstrated that the upregulation of HOXD1 significantly inhibited cell proliferation compared with control cells (P<0.05; Fig. 3B-D). Additionally, to determine cell motility, a wound healing assay was performed. These results demonstrated that HOXD1 overexpression in LUAD cells was associated with a slower wound closure (Fig. 3E). Moreover, Transwell assays showed that the migration and invasion of LUAD cells were inhibited when HOXD1 was upregulated compared with control cells (Fig. 3F).

A549 LV-NC and A549 LV-HOXD1 cells were subcutaneously injected into nude mice and after 28 days, the mice were sacrificed and tumors were dissected. It was demonstrated that the weight of subcutaneous tumors in the HOXD1-upregulated group was lower compared with that in the control group (Fig. 3G). These assays indicated that HOXD1 may potentially have the ability to suppress the progression of LUAD.

HOXD1 promoter undergoes DNA methylation and is associated with the regulation of DNMTs. To investigate the molecular mechanism of low HOXD1 expression levels in LUAD cells, the UALCAN database was used to analyze the methylation level of the HOXD1 promoter region in LUAD samples and normal samples. These results showed that the methylation level of LUAD samples was significantly higher compared

with that of normal samples (Fig. 4A). This indicated that the expression of HOXD1 may be regulated by DNA methylation. CpG islands in the promoter region of the HOXD1 gene were predicted using MethPrimer. These results showed three CpG islands in the upstream 2,000 bp to downstream 1,000 bp of the TSS (Fig. 4B). Furthermore, the methylation level of the HOXD1 promoter in BEAS-2B, A549 and H1299 cells was measured, and the TBS results showed that the total level of methylation was not significantly different in A549 and H1299 cells compared with BEAS-2B cells (Fig. 4C). It is noteworthy that one CpG island in the posterior segment was significantly less methylated, and two CpG islands in the anterior section of this promoter region were significantly more methylated in LUAD cells compared with BEAS-2B cells (Fig. 4D). These findings suggested that in LUAD, the HOXD1 promoter region was regulated by DNA methylation.

The regulation mechanism of HOXD1 hypermethylation was investigated as it was hypothesized that DNMTs were involved in regulating HOXD1 expression in LUAD cells. To determine whether DNMTs were upstream regulators of HOXD1 expression in LUAD cells, A549 cells were treated with the DNMT inhibitor decitabine for 96 h. The mRNA expression level of the HOXD1 gene was detected using RT-qPCR, which demonstrated that DAC significantly increased HOXD1 expression levels in a dose-dependent manner (Fig. 5A). In
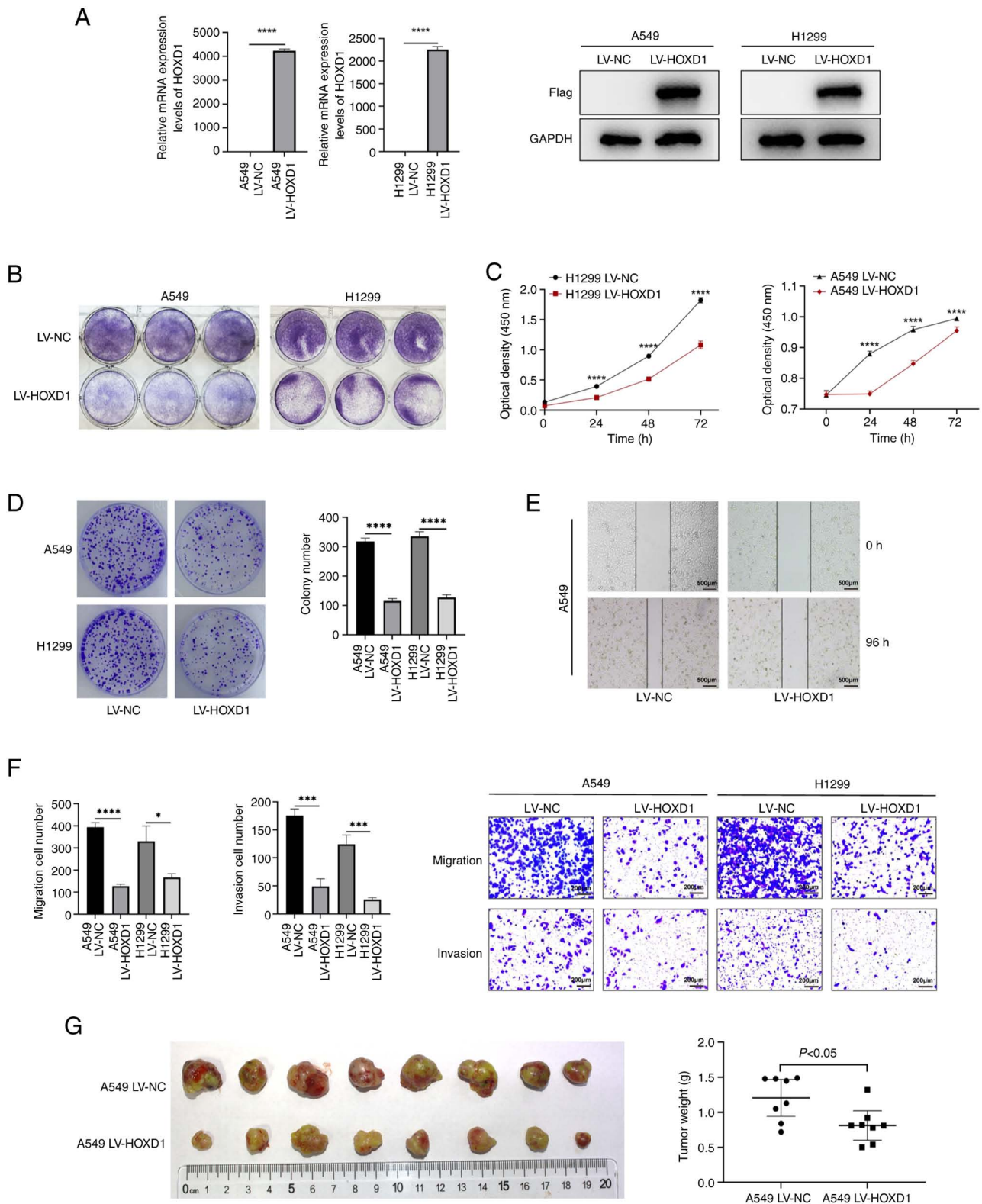
Figure 3. HOXD1 suppressed lung adenocarcinoma progression *in vitro* and *in vivo*. (A) The relative mRNA and protein expression levels of HOXD1 in A549 and H1299 cells were examined using reverse transcription-quantitative PCR and western blotting. Proliferation of A549 and H1299 cells transfected with LV-HOXD1 was evaluated using (B) crystal violet staining, (C) CCK-8 assays and (D) colony formation assays. The cell migration and invasion ability of A549 LV-HOXD1 and H1299 LV-HOXD1 cells were examined using (E) wound healing and (F) Transwell assays. (G) Nude mice were subcutaneously injected with A549 LV-NC and A549 LV-HOXD1 cells and the weight of subcutaneous tumors was measured after 28 days. Data were presented as mean ± SD. *P<0.05, ***P<0.001, ****P<0.0001 vs. NC. HOX, homeobox; LV, lentiviral vector GV492; NC, negative control.

addition, A549 cells were transfected with siRNAs targeting DNMT1, DNMT3A or DNMT3B and a significant increase in HOXD1 expression levels were demonstrated compared with negative controls (Fig. 5B). Furthermore, the 2,000 bp region upstream of the TSS in the HOXD1 promoter region was divided into seven segments, and primers were designed
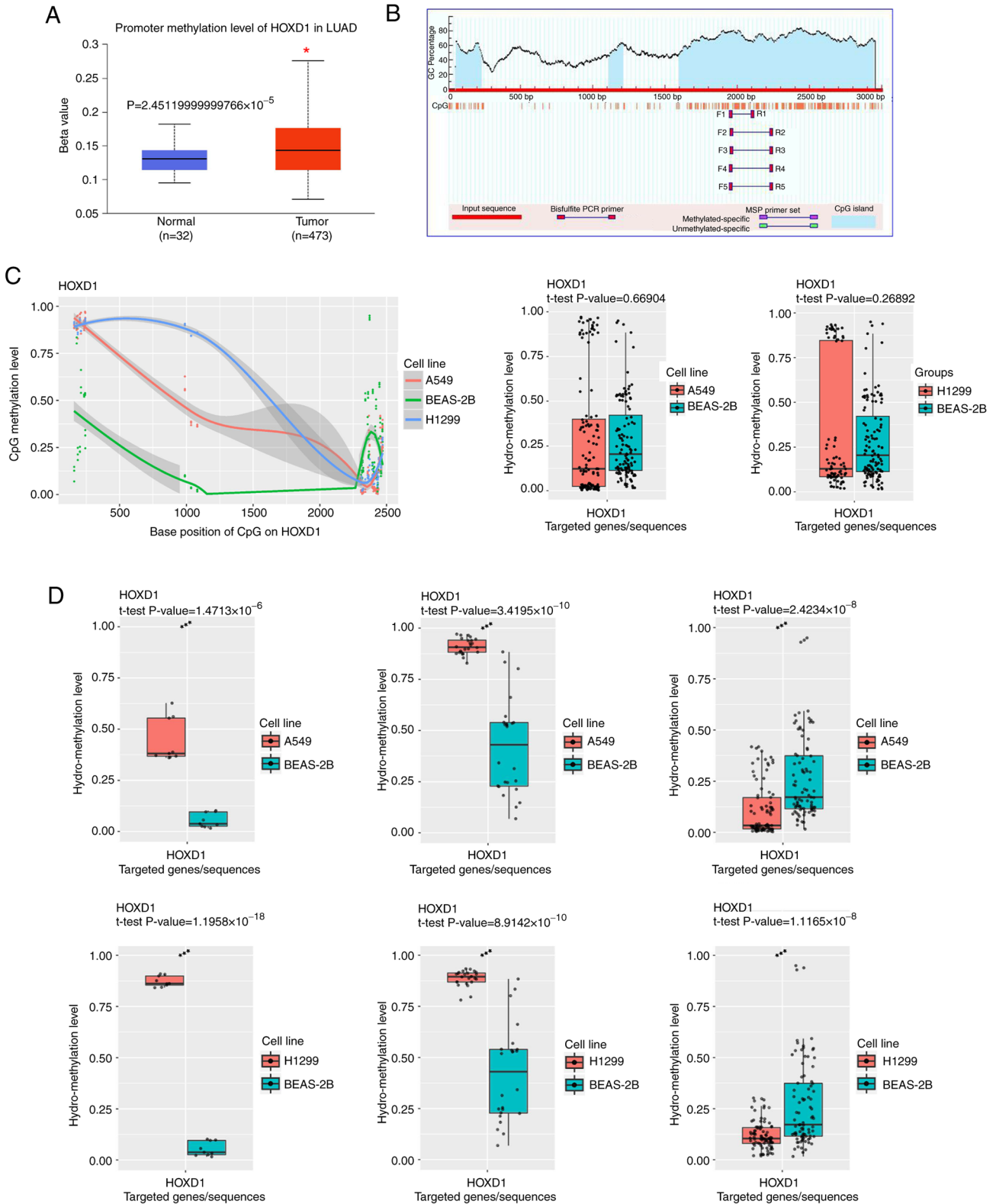
Figure 4. HOXD1 promoter was regulated by DNA methylation. (A) The methylation level of the HOXD1 promoter was examined using The University of Alabama at Birmingham Cancer data analysis Portal database. (B) CpG islands in the promoter region of the HOXD1 gene were predicted by MethPrimer. (C) Total methylation level of the HOXD1 promoter in BEAS-2B, A549 and H1299 cells was assessed using targeted bisulfite sequencing. The shaded area represented the 95% CI. (D) Methylation levels of three CpG islands on the HOXD1 promoter in BEAS-2B, A549 and H1299 cells. Data were presented as mean ± SD. *P<0.05. HOX, homeobox; LUAD, lung adenocarcinoma.

for each segment (Fig. 5C). ChIP-qPCR assays using A549 cells showed that DNMTs bound to the HOXD1 promoter region. DNMT1 combined with F1, F5 and F7 segments of

the HOXD1 promoter (Fig. 5D). DNMT3A combined with F1, F2, F3, F4, F5, F6 and F7 segments of the HOXD1 promoter (Fig. 5E). DNMT3B combined with F1, F2, F3, F4, F5, F6
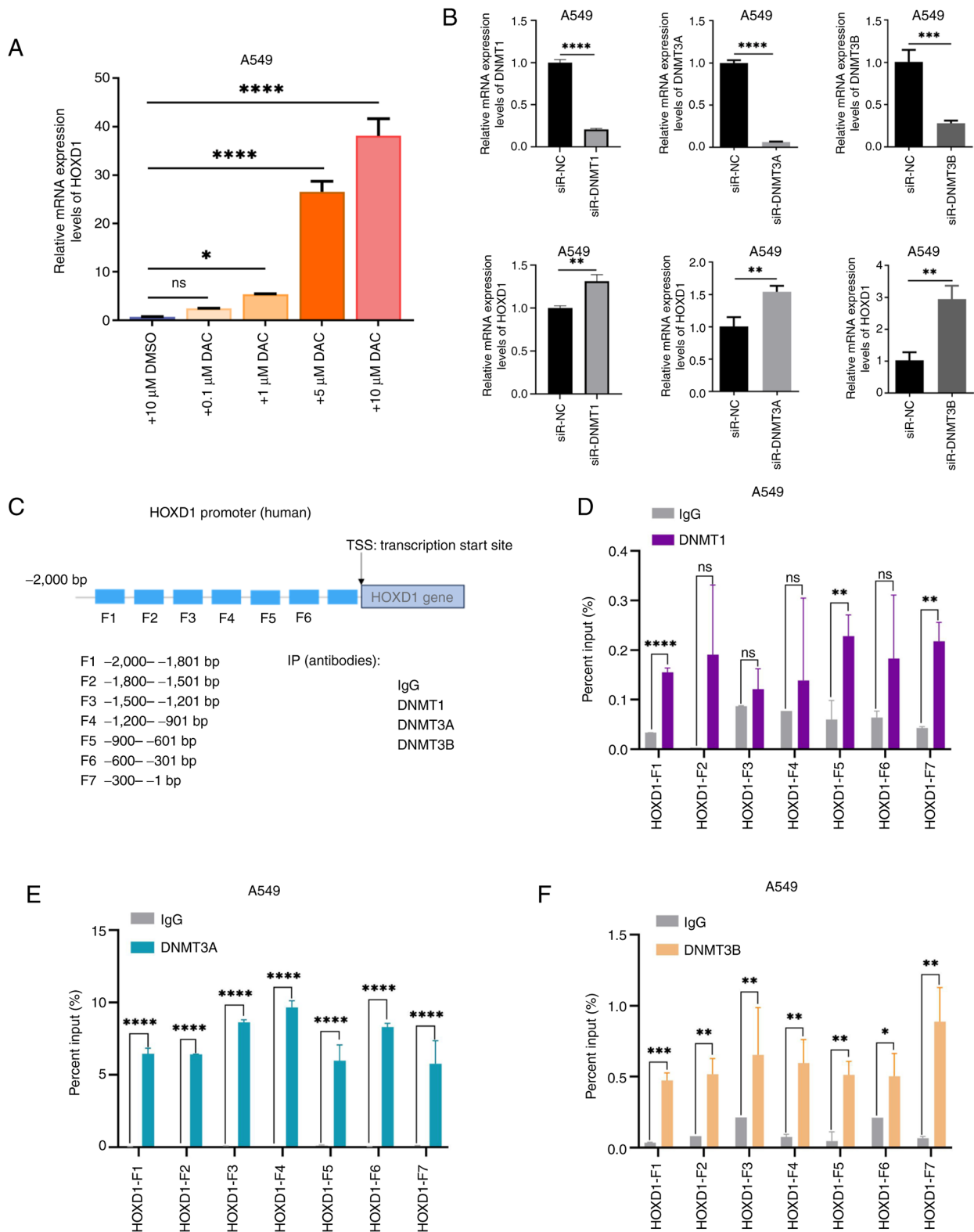
Figure 5. DNMTs targeted the HOXD1 promoter region and led to local hypermethylation. (A) A549 cells were treated with different concentrations of DAC and the mRNA expression levels of HOXD1 were detected using reverse transcription-quantitative PCR. (B) HOXD1 expression was rescued following the transfection of si-DNMTs in A549 cells. (C) Schematic representation of the HOXD1 promoter and ChIP-qPCR primer design. The binding sites of (D) DNMT1, (E) DNMT3A and (F) DNMT3B to the HOXD1 promoter were determined using ChIP-qPCR. Data were presented as mean ± SD. $^*P<0.05$, $^{**}P<0.01$, $^{***}P<0.001$, $^{****}P<0.0001$. HOX, homeobox; DAC, decitabine; si, small interfering RNA; DNMT, DNA methyltransferase; TSS transcription start site; ChIP-qPCR, chromatin immunoprecipitation-quantitative PCR; ns, not significant.

and F7 segments of the HOXD1 promoter (Fig. 5F). These ChIP-qPCR analyses suggested that the HOXD1 promoter region may be enriched with DNMT protein binding. These results suggested that DNMTs target the HOXD1 promoter region and could potentially contribute to local hypermethylation, inducing the dysregulation of HOXD1 in LUAD.
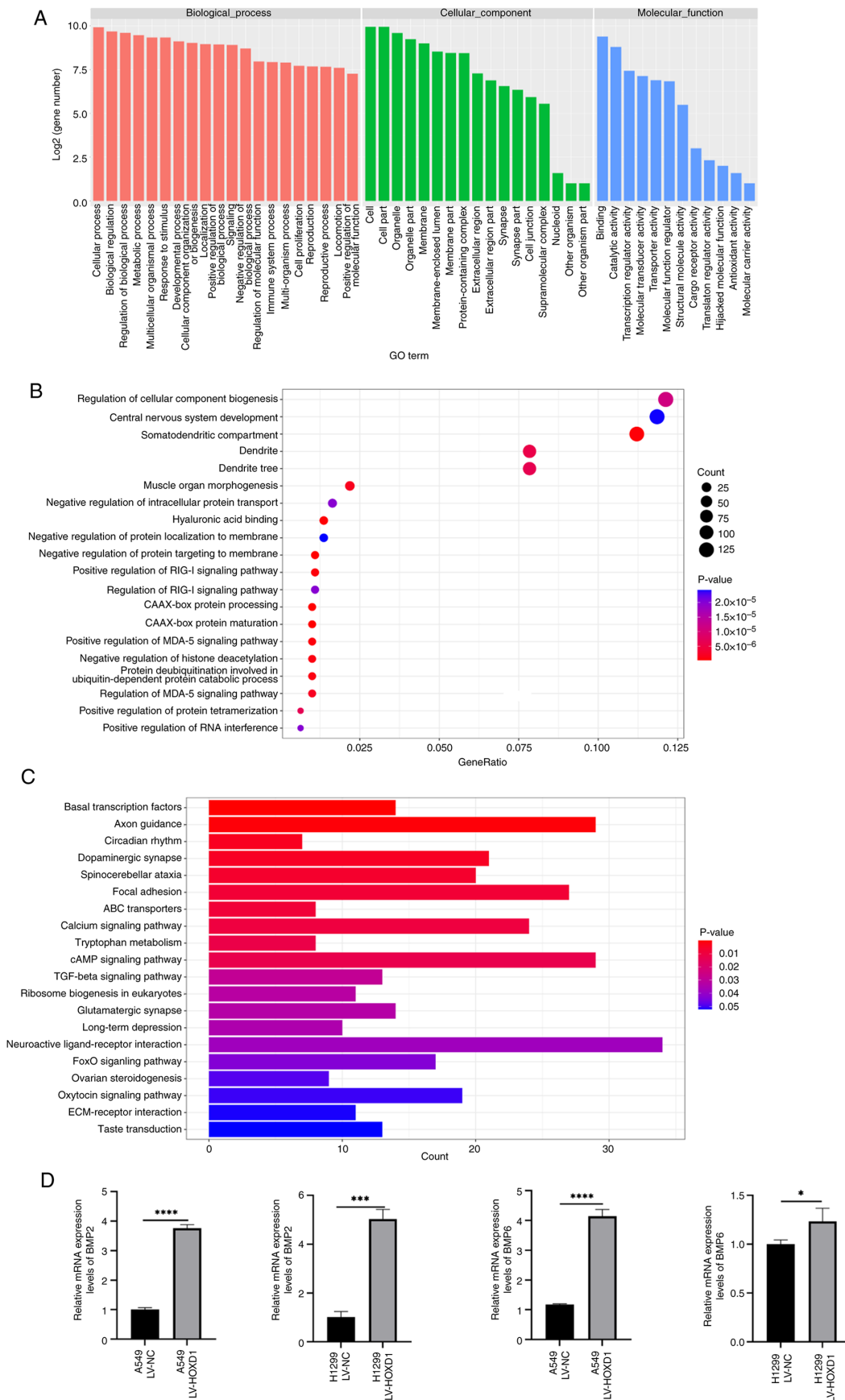
Figure 6. Overexpression of HOXD1 increased the mRNA expression levels of BMP2 and BMP6. Chromatin immunoprecipitation-quantitative PCR was performed to define the downstream regulated by HOXD1. (A) GO clustering map of peak-associated genes according to molecular function, cellular components and biological processes. (B) Bubble map of GO enrichment of peak-associated genes. (C) KEGG-enriched bar graphs for peak-associated genes. (D) The relative mRNA expression levels of BMP2 and BMP6 were detected in A549 LV-HOXD1 and H1299 LV-HOXD1 cells by reverse transcription-quantitative PCR. Data were presented as mean ± SD. *P<0.05, ***P<0.001, ****P<0.0001. HOX, homeobox; BMP, bone morphogenetic protein; GO, Gene Ontology; KEGG, Kyoto Encyclopedia of Genes and Genomes; LV, lentiviral vector GV492; NC, negative control.

Upregulated HOXD1 increases BMP2 and BMP6 transcriptional expression. To better identify the downstream target gene potentially regulated by HOXD1 as a transcription factor in LUAD, ChIP-seq was performed on HOXD1 overexpressing A549 cells to analyze the downstream regulatory network of HOXD1. GO annotation analysis demonstrated that the target sequences of HOXD1 were most enriched in biological processes (Fig. 6A). After the GO enrichment data were sorted according to the P-value, from low to high, the top 20 GO-enriched functions were presented as a bubble graph, which reflected the number of genes and the degree of enrichment of HOXD1-enriched annotations to GO functions. (Fig. 6B). Moreover, following a descending order of P-value for all KEGG enrichment data, bar graphs representing the top 20 KEGG-enriched signaling pathways were created to show the enrichment of HOXD1 in various metabolic pathways (Fig. 6C).

Based on the results of ChIP-seq analysis, 24 genes associated with cellular processes were screened. Then, the expression of these genes was confirmed using RT-qPCR. These results showed that overexpression of HOXD1 elevated the mRNA expression levels of BMP2 and BMP6 (Fig. 6D).

Discussion

The HOX gene family encodes transcription factors that serve a vital role in embryonic development. Studies have also reported a connection between cancer and the abnormal expression of HOX genes (41-43). A subfamily of HOX genes, HOXD, functions as an oncogene or a tumor suppressor that participates in the growth of tumors. Tan *et al* (44) reported that HOXD11 accelerated the development of penile squamous cell carcinoma through degrading the extracellular matrix and promoting epithelial-mesenchymal transition via the fibronectin 1/MMP2/MMP9 pathway. In malignant glioma, decreased miR-7156-3p expression promotes HOXD13 upregulation and induces glioma cell stemness and invasiveness (45). Furthermore, as a tumor suppressor, HOXD8 upregulates serine hydroxymethyltransferase 1 expression and inhibits renal cell carcinoma tumor progression (46). HOXD1 is also recognized as a tumor suppressor gene as it inhibits the progression of renal clear cell carcinoma (47). Hence, the different roles of HOXD in cancer vary depending on the specific cancer type. In the present study, RT-qPCR and western blotting analyses showed that downregulation of HOXD1 was observed in LUAD cell lines. Additionally, low expression levels of HOXD1 were positively correlated with a poor prognosis in patients with LUAD. Moreover, the overexpression of HOXD1 suppressed cancer cell proliferation, migration and invasion in LUAD cells and an animal model. In this regard, HOXD1 could potentially serve as a tumor suppressor gene in LUAD and may be a future promising therapeutic target for anticancer treatment.

A previous study reported that DNA methylation of HOX genes is a common event in cancer (48). The HOXD family is frequently regulated by upstream DNA methylation (49). The methylation level of HOXD3 has been linked to prostate cancer pathology and HOXD3 hypermethylation indicated a poorer prognosis (50). Additionally, hypermethylation of HOXD8 can serve as a biomarker for the identification of biliary tract
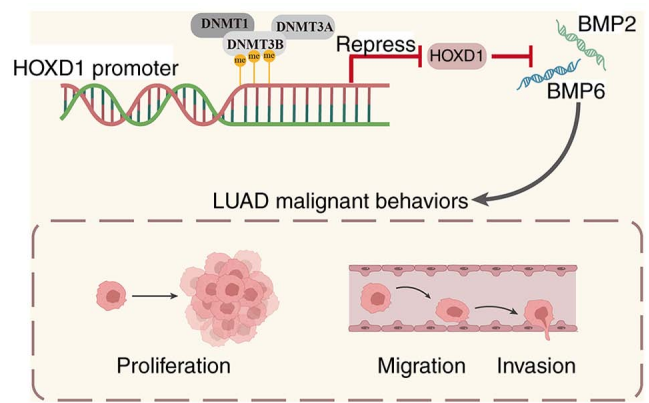

Figure 7. Dysregulated HOXD1-induced LUAD progression. HOX, homeobox; LUAD, lung adenocarcinoma; DNMT, DNA methyltransferase; me, methylation.

cancer (51). Furthermore, methylation of CpG islands at the HOXD locus has also been reported in LUAD (52). Therefore, the present study aimed to explore the upstream regulatory mechanism of HOXD1 in LUAD development. It was demonstrated that DNMTs bind to the HOXD1 promoter region and repress its expression, as shown through bioinformatic analysis and ChIP-qPCR. It was demonstrated that HOXD1 was regulated by DNMTs, through inhibiting or overexpressing DNMTs. Following DNMT inhibition, there was a considerable increase in HOXD1 expression. This suggested that DNMTs over accumulate in the HOXD1 promoter region, thereby repressing HOXD1 expression in LUAD. It is currently unknown how DNMTs regulate the transcriptional expression of HOXD1, and whether other factors are involved in the interactions between DNMTs and HOXD1. Long non-coding RNAs (lncRNAs) have been proposed to serve a significant role in DNA methylation-mediated transcriptional expression regulation of downstream genes (53-55). The potential involvement of lncRNAs in the DNMT-mediated regulation of HOXD1 expression should be analyzed in future studies.

Preliminary downstream mechanistic studies suggested that HOXD1 positively regulates the mRNA expression levels of BMP2 and BMP6, which belong to the TGF-β superfamily (56). Increased TGF-β expression levels in certain types of cancer has been linked to tumor progression and enhanced stem cell characteristics, which allows cancer cells to form tumors and develop resistance to immunotherapy (57). The involvement of BMP in cellular biological processes is primarily mediated through the SMAD and MAPK pathways (58). Previous research on NSCLC has demonstrated that BMP2 is highly expressed in LUAD, while BMP6 expression was not significantly different in NSCLC tissue compared with healthy lung tissue (59). Mechanistically, BMP2 targets downstream PNMA family member 5 to enhance cancer cell migration and invasion (60). Vora *et al* (61) reported that increased BMP2 expression levels cause metabolic dysregulation by suppressing AMP-activated protein kinase expression and upregulating PI3K expression. Moreover, BMP2 can enhance SMAD1/5 phosphorylation, which promotes lung cancer metastasis (62). Furthermore, it has been reported that methylation regulates BMP6 in NSCLC, resulting in epigenetic dysregulation (63). Additionally, it

has been shown that deficiency of BMP6 expression results from increased myosin heavy chain 16 in the advancement of LUAD (64). In the present study, HOXD1, as a transcription factor, regulated the expression levels of BMP2 and BMP6 at the transcriptional level. However, other factors may also be involved in this regulatory progression. Therefore, exploring the binding mechanism between HOXD1 and BMP2 and BMP6, as well as their detailed regulatory relationship with downstream signaling pathways, should be pursued in future research.

In conclusion, the present study demonstrated that HOXD1 was significantly downregulated and HOXD1 functioned as a tumor suppressor in LUAD. DNA methylation-regulated HOXD1 inhibited LUAD progression by increasing BMP2 and BMP6 mRNA expression levels (Fig. 7). These results could potentially provide a theoretical basis for future studies into the early diagnosis and development of novel treatment strategies for NSCLC.

Acknowledgments

Not applicable.

Availability of data and materials

The ChIP sequencing data and target bisulfite sequencing data generated in the present study can be found in the GEO database under accession numbers GSE277213 and GSE277214, respectively, or at the following URLs: https://www.ncbi.nlm.nih.gov/geo/query/acc.cgi?acc=GSE277213 and https://www.ncbi.nlm.nih.gov/geo/query/acc.cgi?acc=GSE277214, respectively.

Authors' contributions

XH, SZ, XZ, HL and YD performed the experiments, analyzed the data and reviewed and edited the manuscript. LL contributed to study conceptualization, methodology, supervision, validation, reviewing and editing. XH and LL confirmed the authenticity of all the raw data. All authors read and approved the final version of the manuscript.

Ethics approval and consent to participate

All animal procedures were approved by the Animal Use and Care Committee at Shandong Provincial Hospital Affiliated with Shandong First Medical University (approval no. 2021-622).

Patient consent for publication

Not applicable.

Competing interests

The authors declare that they have no competing interests.

References

1. Bray F, Laversanne M, Sung H, Ferlay J, Siegel RL, Soerjomataram I and Jemal A: Global cancer statistics 2022: GLOBOCAN estimates of incidence and mortality worldwide for 36 cancers in 185 countries. CA Cancer J Clin 74: 229-263, 2024.
2. Siegel RL, Giaquinto AN and Jemal A: Cancer statistics, 2024. CA Cancer J Clin 74: 12-49, 2024.
3. Bourreau C, Treps L, Faure S, Fradin D and Clere N: Therapeutic strategies for non-small cell lung cancer: Experimental models and emerging biomarkers to monitor drug efficacies. Pharmacol Ther 242: 108347, 2023.
4. Ettinger DS, Wood DE, Aisner DL, Akerley W, Bauman JR, Bharat A, Bruno DS, Chang JY, Chirieac LR, D'Amico TA, *et al*: Non-small cell lung cancer, version 3.2022, NCCN clinical practice guidelines in oncology. J Natl Compr Canc Netw 20: 497-530, 2022.
5. Riely GJ, Wood DE, Ettinger DS, Aisner DL, Akerley W, Bauman JR, Bharat A, Bruno DS, Chang JY, Chirieac LR, *et al*: Non-small cell lung cancer, version 4.2024, NCCN clinical practice guidelines in oncology. J Natl Compr Canc Netw 22: 249-274, 2024.
6. Steens J and Klein D: HOX genes in stem cells: Maintaining cellular identity and regulation of differentiation. Front Cell Dev Biol 10: 1002909, 2022.
7. Jonkers J, Pai P and Sukumar S: Multiple roles of HOX proteins in metastasis: Let me count the ways. Cancer Metastasis Rev 39: 661-679, 2020.
8. Paço A, de Bessa Garcia SA and Freitas R: Methylation in HOX clusters and its applications in cancer therapy. Cells 9: 1613, 2020.
9. Belpaire M, Taminiau A, Geerts D and Rezsohazy R: HOXA1, a breast cancer oncogene. Biochim Biophys Acta Rev Cancer 1877: 188747, 2022.
10. Li L, Zhang X, Liu Q, Yin H, Diao Y, Zhang Z, Wang Y, Gao Y, Ren X, Li J, *et al*: Emerging role of HOX genes and their related long noncoding RNAs in lung cancer. Crit Rev Oncol Hematol 139: 1-6, 2019.
11. Yang R, Zhang G, Dong Z, Wang S, Li Y, Lian F, Liu X, Li H, Wei X and Cui H: Homeobox A3 and KDM6A cooperate in transcriptional control of aerobic glycolysis and glioblastoma progression. Neuro Oncol 25: 635-647, 2023.
12. Bolt CC, Lopez-Delisle L, Mascrez B and Duboule D: Mesomelic dysplasias associated with the HOXD locus are caused by regulatory reallocations. Nat Commun 12: 5013, 2021.
13. Yu M, Zhan J and Zhang H: HOX family transcription factors: Related signaling pathways and post-translational modifications in cancer. Cell Signal 66: 109469, 2020.
14. Hamada J, Omatsu T, Okada F, Furuuchi K, Okubo Y, Takahashi Y, Tada M, Miyazaki YJ, Taniguchi Y, Shirato H, *et al*: Overexpression of homeobox gene HOXD3 induces coordinate expression of metastasis-related genes in human lung cancer cells. Int J Cancer 93: 516-525, 2001.
15. Liu Y, Miao L, Ni R, Zhang H, Li L, Wang X, Li X and Wang J: microRNA-520a-3p inhibits proliferation and cancer stem cell phenotype by targeting HOXD8 in non-small cell lung cancer. Oncol Rep 36: 3529-3535, 2016.
16. Wan K, Shao J, Liu X, Cai Y, Xu Y, Li L, Xiong L and Liang S: HOXD9 contributes to the Warburg effect and tumor metastasis in non-small cell lung cancer via transcriptional activation of PFKFB3. Exp Cell Res 427: 113583, 2023.
17. Li S, Zhang J, Zhao Y, Wang F, Chen Y and Fei X: miR-224 enhances invasion and metastasis by targeting HOXD10 in non-small cell lung cancer cells. Oncol Lett 15: 7069-7075, 2018.
18. Shah N and Sukumar S: The Hox genes and their roles in oncogenesis. Nat Rev Cancer 10: 361-371, 2010.
19. Espín-Pérez A, Brennan K, Ediriwickrema AS, Gevaert O, Lossos IS and Gentles AJ: Peripheral blood DNA methylation profiles predict future development of B-cell Non-Hodgkin Lymphoma. NPJ Precis Oncol 6: 53, 2022.
20. Na F, Pan X, Chen J, Chen X, Wang M, Chi P, You L, Zhang L, Zhong A, Zhao L, *et al*: KMT2C deficiency promotes small cell lung cancer metastasis through DNMT3A-mediated epigenetic reprogramming. Nat Cancer 3: 753-767, 2022.
21. Mancarella D and Plass C: Epigenetic signatures in cancer: Proper controls, current challenges and the potential for clinical translation. Genome Med 13: 23, 2021.
22. Wang J, Yang J, Li D and Li J: Technologies for targeting DNA methylation modifications: Basic mechanism and potential application in cancer. Biochim Biophys Acta Rev Cancer 1875: 188454, 2021.

23. Chen Z and Zhang Y: Role of mammalian DNA methyltransferases in development. Annu Rev Biochem 89: 135-158, 2020.

24. Flausino CS, Daniel FI and Modolo F: DNA methylation in oral squamous cell carcinoma: From its role in carcinogenesis to potential inhibitor drugs. Crit Rev Oncol Hematol 164: 103399, 2021.

25. Zhu L, Tang N, Hang H, Zhou Y, Dong J, Yang Y, Mao L, Qiu Y, Fu X and Cao W: Loss of claudin-1 incurred by DNMT aberration promotes pancreatic cancer progression. Cancer Lett 586: 216611, 2024.

26. Chandrashekar DS, Karthikeyan SK, Korla PK, Patel H, Shovon AR, Athar M, Netto GJ, Qin ZS, Kumar S, Manne U, et al: UALCAN: An update to the integrated cancer data analysis platform. Neoplasia 25: 18-27, 2022.

27. Győrffy B: Integrated analysis of public datasets for the discovery and validation of survival-associated genes in solid tumors. Innovation (Camb) 5: 100625, 2024.

28. Li A, Xie J, Lv L, Zheng Z, Yang W, Zhuo W, Yang S, Cai D, Duan J, Liu P, et al: RPL9 acts as an oncogene by shuttling miRNAs through exosomes in human hepatocellular carcinoma cells. Int J Oncol 64: 58, 2024.

29. Livak KJ and Schmittgen TD: Analysis of relative gene expression data using real-time quantitative PCR and the 2(-Delta Delta C(T)) method. Methods 25: 402-408, 2001.

30. Li LC and Dahiya R: MethPrimer: Designing primers for methylation PCRs. Bioinformatics 18: 1427-1431, 2002.

31. Zuo Y, Zhong J, Bai H, Xu B, Wang Z, Li W, Chen Y, Jin S, Wang S, Wang X, et al: Genomic and epigenomic profiles distinguish pulmonary enteric adenocarcinoma from lung metastatic colorectal cancer. EBioMedicine 82: 104165, 2022.

32. Pu W, Qian F, Liu J, Shao K, Xiao F, Jin Q, Liu Q, Jiang S, Zhang R, Zhang J, et al: Targeted bisulfite sequencing reveals dna methylation changes in zinc finger family genes associated with KRAS mutated colorectal cancer. Front Cell Dev Biol 9: 759813, 2021.

33. Bolger AM, Lohse M and Usadel B: Trimmomatic: A flexible trimmer for Illumina sequence data. Bioinformatics 30: 2114-2120, 2014.

34. Xi Y and Li W: BSMAP: Whole genome bisulfite sequence MAPping program. BMC Bioinformatics 10: 232, 2009.

35. Yachida S, Mizutani S, Shiroma H, Shiba S, Nakajima T, Sakamoto T, Watanabe H, Masuda K, Nishimoto Y, Kubo M, et al: Metagenomic and metabolomic analyses reveal distinct stage-specific phenotypes of the gut microbiota in colorectal cancer. Nat Med 25: 968-976, 2019.

36. Salmon-Divon M, Dvinge H, Tammoja K and Bertone P: PeakAnalyzer: Genome-wide annotation of chromatin binding and modification loci. BMC Bioinformatics 11: 415, 2010.

37. Hull RP, Srivastava PK, D'Souza Z, Atanur SS, Mechta-Grigoriou F, Game L, Petretto E, Cook HT, Aitman TJ and Behmoaras J: Combined ChIP-Seq and transcriptome analysis identifies AP-1/JunD as a primary regulator of oxidative stress and IL-1β synthesis in macrophages. BMC Genomics 14: 92, 2013.

38. Yu G, Wang LG, Han Y and He QY: clusterProfiler: An R package for comparing biological themes among gene clusters. OMICS 16: 284-287, 2012.

39. Ashburner M, Ball CA, Blake JA, Botstein D, Butler H, Cherry JM, Davis AP, Dolinski K, Dwight SS, Eppig JT, et al: Gene ontology: Tool for the unification of biology. The gene ontology consortium. Nat Genet 25: 25-29, 2000.

40. Kanehisa M and Goto S: KEGG: Kyoto encyclopedia of genes and genomes. Nucleic Acids Res 28: 27-30, 2000.

41. Yadav C, Yadav R, Nanda S, Ranga S, Ahuja P and Tanwar M: Role of HOX genes in cancer progression and their therapeutical aspects. Gene 919: 148501, 2024.

42. Morgan R, Hunter K and Pandha HS: Downstream of the HOX genes: Explaining conflicting tumour suppressor and oncogenic functions in cancer. Int J Cancer 150: 1919-1932, 2022.

43. Paco A, Aparecida de Bessa Garcia S, Leitao Castro J, Costa-Pinto AR and Freitas R: Roles of the HOX proteins in cancer invasion and metastasis. Cancers (Basel) 13: 10, 2020.

44. Tan X, Liu Z, Wang Y, Wu Z, Zou Y, Luo S, Tang Y, Chen D, Yuan G and Yao K: miR-138-5p-mediated HOXD11 promotes cell invasion and metastasis by activating the FN1/MMP2/MMP9 pathway and predicts poor prognosis in penile squamous cell carcinoma. Cell Death Dis 13: 816, 2022.

45. Zhang J, Deng M, Tong H, Xue W, Guo Y, Wang J, Chen L and Wang S: A novel miR-7156-3p-HOXD13 axis modulates glioma progression by regulating tumor cell stemness. Int J Biol Sci 16: 3200-3209, 2020.

46. Yang Y, Zhang M, Zhao Y, Deng T, Zhou X, Qian H, Wang M, Zhang C, Huo Z, Mao Z, et al: HOXD8 suppresses renal cell carcinoma growth by upregulating SHMT1 expression. Cancer Sci 114: 4583-4595, 2023.

47. Wang L, Wang X, Sun H, Wang W and Cao L: A pan-cancer analysis of the role of HOXD1, HOXD3, and HOXD4 and validation in renal cell carcinoma. Aging (Albany NY) 15: 10746-10766, 2023.

48. Hu X, Wang Y, Zhang X, Li C, Zhang X, Yang D, Liu Y and Li L: DNA methylation of HOX genes and its clinical implications in cancer. Exp Mol Pathol 134: 104871, 2023.

49. Wang L, Qiao C, Cao L, Cai S, Ma X, Song X, Jiang Q, Huang C and Wang J: Significance of HOXD transcription factors family in progression, migration and angiogenesis of cancer. Crit Rev Oncol Hematol 179: 103809, 2022.

50. Kron KJ, Liu L, Pethe VV, Demetrashvili N, Nesbitt ME, Trachtenberg J, Ozcelik H, Fleshner NE, Briollais L, van der Kwast TH and Bapat B: DNA methylation of HOXD3 as a marker of prostate cancer progression. Lab Invest 90: 1060-1067, 2010.

51. Loi E, Zavattari C, Tommasi A, Moi L, Canale M, Po A, Sabato C, Vega-Benedetti AF, Ziranu P, Puzzoni M, et al: HOXD8 hypermethylation as a fully sensitive and specific biomarker for biliary tract cancer detectable in tissue and bile samples. Br J Cancer 126: 1783-1794, 2022.

52. Shiraishi M, Sekiguchi A, Oates AJ, Terry MJ and Miyamoto Y: HOX gene clusters are hotspots of de novo methylation in CpG islands of human lung adenocarcinomas. Oncogene 21: 3659-3662, 2002.

53. Huang W, Li H, Yu Q, Xiao W and Wang DO: LncRNA-mediated DNA methylation: An emerging mechanism in cancer and beyond. J Exp Clin Cancer Res 41: 100, 2022.

54. Geng X, Zhao J, Huang J, Li S, Chu W, Wang WS, Chen ZJ and Du Y: lnc-MAP3K13-7:1 inhibits ovarian GC proliferation in PCOS via DNMT1 downregulation-mediated CDKN1A promoter hypomethylation. Mol Ther 29: 1279-1293, 2021.

55. Xu SF, Zheng Y, Zhang L, Wang P, Niu CM, Wu T, Tian Q, Yin XB, Shi SS, Zheng L and Gao LM: Long non-coding RNA LINC00628 interacts epigenetically with the LAMA3 promoter and contributes to lung adenocarcinoma. Mol Ther Nucleic Acids 18: 166-182, 2019.

56. Wakefield LM and Hill CS: Beyond TGFβ: Roles of other TGFβ superfamily members in cancer. Nat Rev Cancer 13: 328-341, 2013.

57. Derynck R, Turley SJ and Akhurst RJ: TGFβ biology in cancer progression and immunotherapy. Nat Rev Clin Oncol 18: 9-34, 2021.

58. Massagué J and Sheppard D: TGF-β signaling in health and disease. Cell 186: 4007-4037, 2023.

59. Langenfeld EM, Bojnowski J, Perone J and Langenfeld J: Expression of bone morphogenetic proteins in human lung carcinomas. Ann Thorac Surg 80: 1028-1032, 2005.

60. Huang F, Cao Y, Wang C, Lan R, Wu B, Xie X, Hong J, Fu L and Wu G: PNMA5 promotes bone metastasis of non-small-cell lung cancer as a target of BMP2 signaling. Front Cell Dev Biol 9: 678931, 2021.

61. Vora M, Mondal A, Jia D, Gaddipati P, Akel M, Gilleran J, Roberge J, Rongo C and Langenfeld J: Bone morphogenetic protein signaling regulation of AMPK and PI3K in lung cancer cells and C. elegans. Cell Biosci 12: 76, 2022.

62. Wu CK, Wei MT, Wu HC, Wu CL, Wu CJ, Liaw H and Su WP: BMP2 promotes lung adenocarcinoma metastasis through BMP receptor 2-mediated SMAD1/5 activation. Sci Rep 12: 16310, 2022.

63. Kraunz KS, Nelson HH, Liu M, Wiencke JK and Kelsey KT: Interaction between the bone morphogenetic proteins and Ras/MAP-kinase signalling pathways in lung cancer. Br J Cancer 93: 949-952, 2005.

64. Zhang L, Liu J, Wang H, Xu Z, Wang Y, Chen Y and Peng H: MYH16 upregulation is associated with lung adenocarcinoma aggressiveness and immune infiltration. J Biochem Mol Toxicol 37: e23490, 2023.